Lithium Storage

DOI: 10.1002/anie.200803420

Reversible Storage of Lithium in a Rambutan-Like Tin–Carbon Electrode

*Da Deng and Jim Yang Lee**

Nanomaterials can be fabricated into a variety of morphological forms (e.g. nanospheres, nanocubes, nanoboxes, nanorods, nanotubes, nanowires, and nanobelts),[1–7] however, reports on autonomous organization of these basic nanoscale building blocks into extended structures are still rare. Nanopatterns are often generated using expensive, templated, or lithography approaches.[8–11] The ability to form complex nanostructures from materials of different origins and with different geometrical attributes by self-assembly processes is more preferable and cost-effective, but it also presents significant challenges.

The interest in composite nanostructured materials is driven by the possibility of combining different indigenous material properties in a complementary manner to enhance their performances for variety of applications.[12–14] In energy-storage applications, nanostructured composites of carbon and tin have been proposed as a high capacity substitute for the carbon anode of lithium ion batteries.[13,15–23] The theoretical specific capacity of tin (992 $mA\,h\,g^{-1}$) is considerably higher than that of graphite (350 $mAh\,g^{-1}$ nominal), however, the high capacity is never realized in practice because of a pulverization-induced capacity fading that is caused by huge specific-volume changes during the insertion and extraction of the lithium ions. It is believed that a carefully crafted composite of tin and carbon on the nanoscale may solve the poor cyclability of the tin electrodes.[16,18,19,21–23]

Herein we report a simple procedure to fabricate a rambutan-like tin–carbon (Sn@C) nanocomposite from three basic construction units: tin-containing carbon mesospheres, carbon nanotubes with completely or partially filled tin interiors, and carbon-coated pear-shaped tin nanoparticles ("nanopears"). The synthesis of the rambutan-like (a rambutan is a tropical fruit) carbon–tin nanocomposite is outlined in Scheme 1.

The rambutan-like morphology of the Sn@C nanocomposite can be seen in the field emission scanning electron microscope (FESEM) images taken at different magnifications (Figure 1 a and b). The hair-like structure on the surface of the mesospheres resembles that of a tropical fruit rambutan (Supporting Information, Figure S1). The enlarged view of the mesosphere shows that the hair-like structure is made up of nanorods and nanopears with roots in the surface layer (Figure 1 b). The rambutan-like architecture was also confirmed by low magnification scanning tunneling electron microscope (STEM; Figure 1 c). The distribution of nanorods and nanopears was uniform across the particle surface. Based on our previous study,[24] the product of the solvothermal synthesis are carbon mesospheres with embedded SnO_2 nanoparticles. In the subsequent step of chemical vapor deposition, SnO_2 nanoparticles in the carbon mesospheres

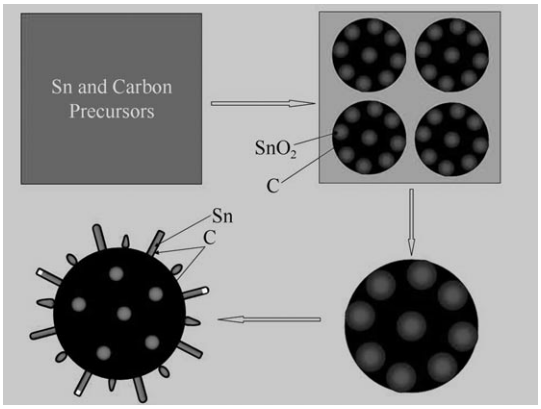

Scheme 1. Procedures for the fabrication of the rambutan-like Sn@C nanoarchitecture.

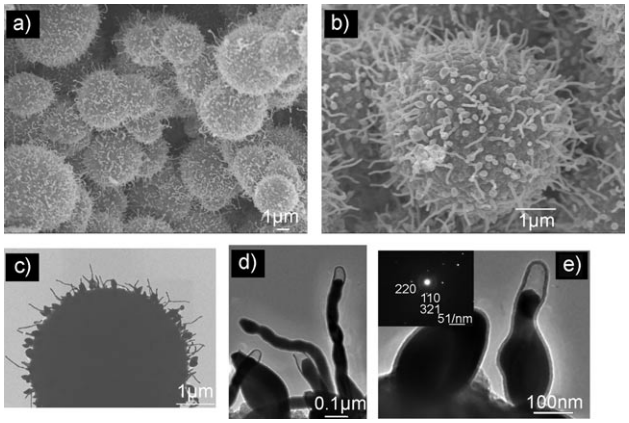

Figure 1. FESEM images of the rambutan-like nanoarchitecture at a) low and b) high magnifications. c) STEM images of the Rambutan-like nanostructure at low magnification, d) magnified TEM view of the hairs showing carbon nanotubes with completely filled and partially filled tin interiors and carbon-coated tin nanopears. e) TEM images of a nanopear, and the growth of a nanopear into a tin nanorod that is surrounded by a carbon mantle. Inset: SAED pattern of a tin nanorod surrounded by a carbon mantle.

[*] D. Deng, Prof. J. Y. Lee
Department of Chemical & Biomolecular Engineering
National University of Singapore
10 Kent Ridge Crescent, Singapore 119260 (Singapore)
Fax: (+65) 6779-1936
E-mail: cheleejy@nus.edu.sg

Supporting information for this article is available on the WWW under http://dx.doi.org/10.1002/anie.200803420.

were reduced to metallic tin nanoparticles. The dispersion of tin nanoparticles throughout the volume of the carbon mesospheres is evident in the FESEM image of a broken carbon mesosphere (Supporting Information, Figure S2a), and confirmed by TEM images (Supporting Information, Figure S2b). The hair-like structure consists of carbon tubes that are completely filled or partially filled with tin, and carbon-coated tin nanopears. The magnified view of the nanorods and nanopears on the carbon mesosphere surface shows a core–shell structure consisting of a shell of thin carbon layers over a core that is a metallic tin nanorod or tin nanopear (Figure 1 d, e; Supporting Information, Figure S3). The single-crystalline nature of the tin core inside the carbon mantle was confirmed by the selected area electron diffraction (SAED) pattern (inset of Figure 1 e), in which diffraction spots confirmed the presence of crystalline tin and the very weak diffraction ring of carbon (002) was detected (d(002) of about 3.5 nm). The carbon shell of these hair-like structure was about 9 nm in thickness, corresponding to 25 layers of short graphene sheets aligned co-axially as shown in the high resolution transmission electron microscope (HRTEM) image of the wall area (Supporting Information, Figure S3d). The d(002) spacing of the carbon walls measured from the HRTEM was about 0.35 nm, and is consistent with the SAED measurement. The slightly expanded d(002) spacing compared to that of graphite (0.34 nm) is an indication of low carbon crystallinity, which can facilitate diffusion of lithium ions through the walls of the carbon nanotubes.[25] Furthermore, TEM images of the hair-like structure shows that the nanorods developed from the nanopears (Supporting Information, Figure S3 a, b).

At the temperature of 700 °C, which is required for the chemical vapor deposition (CVD), the net reducing environment provided by acetylene and carbon mesospheres, was sufficient for the reduction of SnO_2 to metallic tin.[26] The presence of metallic tin was confirmed by the X-ray diffraction (XRD) analysis of the Sn@C nanocomposite (Figure 2 a). All the peaks in the diffractogram could be indexed to crystalline metallic tin according to JCPDS card No. 04-0673. No peaks attributable to SnO_2 were observed, indicating high phase purity of the product. The sharp diffraction peaks also indicated good crystallinity of the tin phase. Graphitic carbon diffraction at about 26° was virtually undetectable, suggesting that the carbon phase was mainly amorphous, and the carbon nanotubes encapsulating the tin nanrods or tin nanopears were short graphene sheets lacking long-range order. The energy dispersive X-ray spectroscopy (EDX) pattern shows the exclusive presence of carbon and tin (Figure 2 b). The absence of oxygen in the EDX pattern is consistent with XRD determination, further confirming that SnO_2 had been completely reduced to metallic tin. The tin content in the rambutan-like Sn@C composite as estimated by thermogravimetric analysis (TGA) was 23 % by weight (Supporting Information, Figure S4).

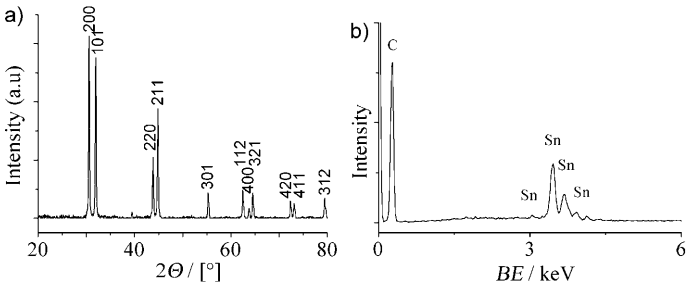

Figure 2. a) XRD and b) EDX patterns of the rambutan-like Sn@C nanocomposite.

The presence of the hair-like structures on the carbon mesosphere surface is the principal feature of the rambutan-like nanoarchitecture and a slightly modified "base-growth" model may be used to rationalize its growth. As tin has relatively low melting point (232 °C) and high boiling point (2270 °C), the metallic tin, during the process of reduction from SnO_2, could easily coalesce to form liquid tin droplets on the carbon mesosphere surface under the high reaction temperature of 700 °C. The tin droplets then serve as the catalyst for the decomposition of the acetylene gas and the deposition of carbon.[27] The emergence of carbon nanotubes by the modified "base growth" model is shown in Scheme 2.

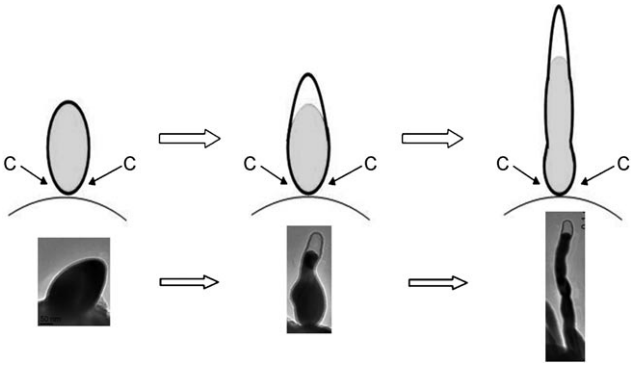

Scheme 2. A modified "base growth" model for the formation of carbon encapsulation that surrounds the metallic tin nanorods, and the corresponding TEM images.

Carbon that was formed during the decomposition of the acetylene gas was first deposited on the surface of the tin droplets followed by dissolution into the metallic tin. After the solubility of carbon in tin was exceeded (carbon dissolves only sparingly in tin),[27] the carbon deposition started forming a shell surrounding the droplets of the metallic tin particles. Owing to the anisotropic property of the carbon shell, which tends to grow into tubular structures with additional supplies of carbon, the carbon encapsulating the tin droplet evolved into a pear-shaped structure before it was developed fully into the final tubular structure. The tin catalyst in this case was in the liquid state and thus the method is different from a typical "base-growth".[28] Along with the growth of the carbon nanotubes, capillary forces would draw additional molten tin into the nanotubes,[20] filling the interiors of these nanotubes to different degrees, and eventually forming the tin nanorods that are encapsulated in a thin carbon mantle (Figure 1 d and Figure S3 in the Supporting Information). The metallic tin inside the carbon nanotubes (the carbon mantle)

could be re-liquified upon prolonged exposure to the electron beam, as shown by the movable boundaries detected in a series of TEM images taken in succession (Supporting Information, Figure S5).

The hierarchical Rambutan-like Sn@C nanocomposite was tested for reversible lithium storage and the results of the first two cycles of charging (lithiation) and discharging (de-lithiation) are presented in the inset of the Figure 3a. The

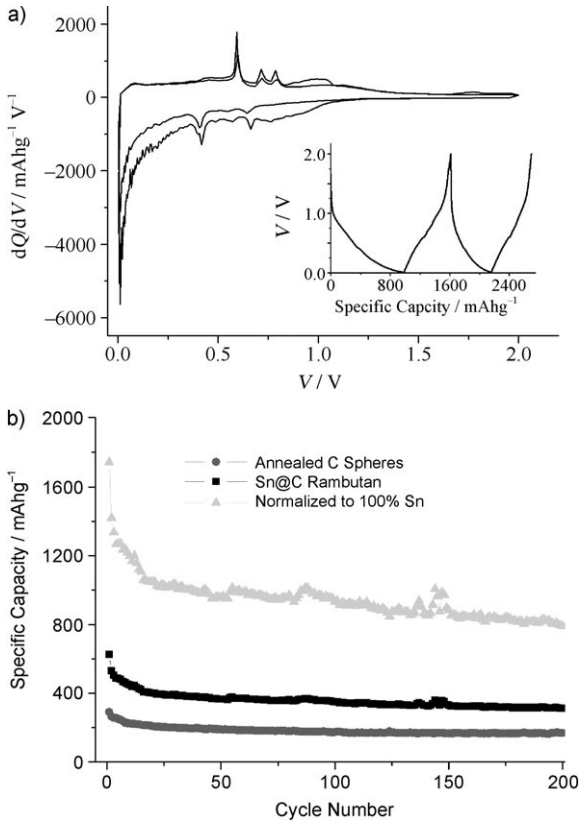

Figure 3. a) Differential charge–discharge capacity plots for the first two cycles. The first two cycles of galvanostatic charge and discharge curves are provided in the inset. b) Cyclability of annealed carbon mesospheres, rambutan-like Sn@C composite, and the Sn phase in the nanocomposite. Test conditions: current density of 100 mA g^{-1} in the voltage window of 5 mV–2 V.

corresponding charge–discharge differential capacity plots are shown in Figure 3a. The two reduction peaks at 0.41 V and 0.66 V in the first cycle can be assigned to the alloying reaction between lithium and tin forming Li_xSn alloys.[16,19] The irreversible broad peak around 0.8 V is assigned to the formation of solid electrolyte interphase (SEI) on the carbon surface as a result of the reductive decomposition of the electrolyte, which contributes to the irreversible capacity loss during the first cycle.[19] The absence of irreversible peaks due to catalytic decomposition of the electrolyte on metallic Sn (at 1.05 V and 1.55 V typically) indicates that Sn was not exposed to the electrolyte.[19] The distinctive oxidization peaks at 0.6 V, 0.72 V, and 0.78 V in the first discharge cycles can be assigned to the de-alloying reaction of Li_xSn. The unabated intensity of these peaks in subsequent cycles indicates a good electrochemical reversibility of the tin.[16,18,19]

The Rambutan-like tin-carbon nanocomposites electrode cycled very well, as shown in Figure 3b. Indeed after 200 cycles the capacity (311 mAh g^{-1}) was still comparable to the nominal capacity of a graphite anode, although in this case the carbon phase (77%) was poorly graphitized (carbon formed during a low temperature carbonization process). The lithium storage properties of the poorly graphitized carbon matrix[*] were determined independently to be 168 mAh g^{-1} in the 200th cycle. Subtracting the contribution of the carbon matrix in the Sn@C composite, a capacity of 790 mAh g^{-1}, or circa 80% of the theoretical value of Sn, could be determined for the 23wt% of encapsulated Sn on a Sn-only basis. Such impressive reversibility for lithium storage should make tin as a suitable material for lithium storage. On the other hand, the electrochemical performance of the product of solvothermal synthesis and annealed product without the subsequent CVD treatment (SnO_2 and Sn/SnO_2 containing carbon mesospheres) was significantly lower (Supporting Information, Figure S7b). The CVD treatment was essential to the development of the Rambutan-like structures, whose one dimensional "hair-like" structures can be potentially advantageous for electrical connectivity. Improvements could also arise from the encapsulation of metallic tin in a soft carbon phase, which worked effectively against the aggregation of nanosized tin. However, with a tin loading of only 23wt% in a low-graphitized carbon matrix, the overall capacity was relatively low. Raising the tin loading and improving the graphitization of carbon in the nanocomposite are our ongoing efforts.

In summary, we have fabricated a hierarchical Sn@C composite nanostructure consisting of tin-containing carbon mesospheres, carbon nanotubes with completely-filled or partially-filled metallic tin interiors, and carbon encapsulated tin nanopears by a simple two-step procedure. The molten tin droplets present on the carbon mesosphere surface from SnO_2 reduction under the experimental conditions were responsible for the formation of hair-like structures in the rambutan architecture by means of a modified "base growth" mechanism. The improved electrochemical performance of tin in the nanocomposites can be attributed to the unique Sn@C structure, which prevents the aggregation of nanosized metallic tin and the presence of one-dimensional carbon nanotube "hair-like" structures which may enhance the electrical connectivity and integration of the active electrode materials.

Experimental Section

In a typical experiment, $SnCl_4$ (4 mmol) and D-glucose (10 mmol) monohydrate were dissolved in a mixture of water (5 mL) and ethanol (30 mL). The clear solution was transferred to a teflon-lined autoclave and sealed. The autoclave was heated to 180°C and kept at this temperature for 24 h to form SnO_2-containing carbon mesospheres.[24] The solvothermally formed SnO_2-containing carbon mesospheres after recovery were placed in a quartz combustion boat inside a tube furnace where chemical vapor deposition took place by using a

[*] Using annealed carbon mesospheres from the hydrothermal carbonization of glucose.

flowing mixture of 10% acetylene and 90% N_2 for 4 h (200 standard cubic centimeters per minute (sccm)) at 700°C.[25] The product recovered at the end of the procedure was characterized by FESEM, STEM, TEM, HRTEM, XRD, EDX, and TGA. The lithium storage properties were measured by the electrochemical methods described elesewhere.[24,25]

Received: July 15, 2008
Published online: January 20, 2009

Keywords: carbon · lithium storage · lithium-ion batteries · tin oxide · tin

[1] Y. D. Yin, R. M. Rioux, C. K. Erdonmez, S. Hughes, G. A. Somorjai, A. P. Alivisatos, *Science* **2004**, *304*, 711.
[2] D. D. D. Ma, C. S. Lee, F. C. K. Au, S. Y. Tong, S. T. Lee, *Science* **2003**, *299*, 1874.
[3] Y. G. Sun, Y. N. Xia, *Science* **2002**, *298*, 2176.
[4] W. U. Huynh, J. J. Dittmer, A. P. Alivisatos, *Science* **2002**, *295*, 2425.
[5] Z. W. Pan, Z. R. Dai, Z. L. Wang, *Science* **2001**, *291*, 1947.
[6] P. Poizot, S. Laruelle, S. Grugeon, L. Dupont, J. M. Tarascon, *Nature* **2000**, *407*, 496.
[7] P. M. Ajayan, S. Iijima, *Nature* **1992**, *358*, 23.
[8] Z. L. Wang, J. H. Song, *Science* **2006**, *312*, 242.
[9] J. Li, H. C. Zeng, *Angew. Chem.* **2005**, *117*, 4416; *Angew. Chem. Int. Ed.* **2005**, *44*, 4342.
[10] B. Liu, H. C. Zeng, *J. Am. Chem. Soc.* **2004**, *126*, 16744.
[11] J. Yang, H. I. Elim, Q. B. Zhang, J. Y. Lee, W. Ji, *J. Am. Chem. Soc.* **2006**, *128*, 11921.
[12] H. Shen, J. Tan, W. M. Saltzman, *Nat. Mater.* **2004**, *3*, 569.
[13] A. S. Aricò, P. Bruce, B. Scrosati, J. M. Tarascon, W. Van Schalkwijk, *Nat. Mater.* **2005**, *4*, 366.
[14] R. Bashyam, P. Zelenay, *Nature* **2006**, *443*, 63.
[15] Y. Idota, T. Kubota, A. Matsufuji, Y. Maekawa, T. Miyasaka, *Science* **1997**, *276*, 1395.
[16] M. Winter, J. O. Besenhard, *Electrochim. Acta* **1999**, *45*, 31.
[17] J. M. Tarascon, M. Armand, *Nature* **2001**, *414*, 359.
[18] K. T. Lee, Y. S. Jung, S. M. Oh, *J. Am. Chem. Soc.* **2003**, *125*, 5652.
[19] Y. S. Jung, K. T. Lee, J. H. Ryu, D. Im, S. M. Oh, *J. Electrochem. Soc.* **2005**, *152*, A1452.
[20] C. Guerret-Piécourt, Y. Lebouar, A. Loiseau, H. Pascard, *Nature* **1994**, *372*, 761.
[21] G. Derrien, J. Hassoun, S. Panero, B. Scrosati, *Adv. Mater.* **2007**, *19*, 2336.
[22] B. K. Guo, J. Shu, K. Tang, Y. Bai, Z. X. Wang, L. Q. Chen, *J. Power Sources* **2008**, *177*, 205.
[23] W. M. Zhang, J. S. Hu, Y. G. Guo, S. F. Zheng, L. S. Zhong, W. G. Song, L. J. Wan, *Adv. Mater.* **2008**, *20*, 1160.
[24] D. Deng, J. Y. Lee, *Chem. Mater.* **2008**, *20*, 1841.
[25] D. Deng, J. Y. Lee, *Chem. Mater.* **2007**, *19*, 4198.
[26] L. Janković, D. Gourins, P. N. Trikalitis, I. Arfaoi, T. Cren, P. Rudolf, M-H. Sage, T. T.M. Palstra, B. Kooi, J. De Hosson, M. A. Karakassides, K. Dimos, A. Moukarika, T. Bakas, *Nano Lett.* **2006**, *6*, 1131.
[27] R. Y. Li, X. C. Sun, X. R. Zhou, M. Cai, X. L. Sun, *J. Phys. Chem. C* **2007**, *111*, 9130.
[28] M. Lin, J. P. Y. Tan, C. Boothroyd, K. P. Loh, E. S. Tok, Y. L. Foo, *Nano Letters* **2006**, *6*, 449.

